Progress in Physics of Applied Materials 7 (2027), Serial Number 14, 27-36

Semnan University

Progress in Physics of Applied Materials

journal homepage: https://ppam.semnan.ac.ir/

Quantum Chemical Investigation of Structural, Spectroscopic, Electronic and Nonlinear Optical Properties of Gefitinib Using DFT

Atul Kumar Shukla[a], Anchal Srivastava[a], Sunil Kumar Mishra[b] ,Mritunjai Mishra[c], Nitin Dwivedi[a], R K Shukla[a]*

[a]*Department of Physics,University of Lucknow, Lucknow-226007, India*
[b]*Department of Chemistry,M. L. K. (PG) College, Balrampur, Uttar Pradesh, India*
[c]*Department of Physics,Siddharth University, Siddharthnagar, Uttar Pradesh, India*

ARTICLE INFO

Article history:
Received: 15 April 2026
Revised: 22 Nay 2026
Accepted: 5 June 2026
Published online: 14 July 2026

Keywords:
Density Functional Theory (DFT);
Gefitinib;
Vibrational Spectroscopy;
Frontier Molecular Orbitals;
Molecular Electrostatic Potential;
Density of States;
Nonlinear Optical Properties;
Non-Covalent Interactions.

ABSTRACT

Gefitinib, a well-known epidermal growth factor receptor (EGFR) tyrosine kinase inhibitor used in the treatment of non-small cell lung cancer, was investigated in this study using density functional theory (DFT). The molecular structure was optimized at the B3LYP/6-311G(d,p) level of theory, and the absence of imaginary frequencies confirmed the stability of the optimized structure. Vibrational analysis provided detailed insight into the characteristic functional groups of the molecule. The electronic properties were analyzed using frontier molecular orbital analysis. The HOMO and LUMO energies were calculated to be −6.0734 eV and −1.8243 eV, respectively, with an energy gap of 4.2491 eV, indicating the good kinetic stability of the molecule. TD-DFT studies demonstrated a main absorption band at approximately 325 nm, which was mainly attributed to π → π* electronic transitions in the conjugated quinazoline framework. Solvent-phase analysis using the PCM model revealed a slight red shift in the absorption wavelength, confirming the effect of solvation on the electronic excitation characteristics of gefitinib. The calculated nonlinear optical parameters showed significant polarizability and first hyperpolarizability values, which can be attributed to effective intramolecular charge transfer and extended π-conjugation.

1. Introduction

Cancer is a leading cause of death worldwide [1]. Non-small cell lung cancer (NSCLC) accounts for roughly 85% of lung cancer cases [2]. Conventional chemotherapy often lacks selectivity and causes significant side effects, which has motivated the development of targeted therapies that attack specific molecular mechanisms in tumors. One such mechanism is the epidermal growth factor receptor (EGFR) signaling pathway, which is frequently overactive in NSCLC. Gefitinib is a selective EGFR tyrosine kinase inhibitor that blocks this pathway [3]. It is FDA-approved for patients with metastatic NSCLC harboring activating EGFR mutations [4] and is listed on the WHO Essential Medicines List [5], underscoring its clinical importance. By inhibiting mutated EGFR, gefitinib can suppress the growth of these tumor cells, improving patient outcomes compared with standard chemotherapy.

Computational chemistry offers powerful tools for understanding drug molecules at the atomic level. Density functional theory (DFT) has become a standard method for predicting the structure, spectra, and electronic properties of complex organic compounds. Numerous DFT studies have investigated small-molecule therapeutics to reveal their stability, reactivity, and optical behavior [6]. However, to our knowledge, a complete quantum-chemical analysis of gefitinib has not been reported. In particular, its nonlinear optical (NLO) response and noncovalent interaction (NCI) characteristics remain

* Corresponding author.
E-mail address: rajeshkumarshukla00@gmail.com

Cite this article as:

Shukla, A.K., Srivastava, A., Mishra, S.K., Mishra, M., Dwivedi, N., Shukla, R.K., 2027. Quantum Chemical Investigation of Structural, Spectroscopic, Electronic and Nonlinear Optical Properties of Gefitinib Using DFT. *Progress in Physics of Applied Materials*, *7*(1), pp.27-36. DOI: 10.22075/ppam.2026.40899.1215

unexplored, despite their potential relevance to material applications.

Addressing this gap, a detailed DFT investigation of the gefitinib molecule was conducted at the B3LYP/6-311G(d,p) level of theory in this study. The resulting optimized molecular geometry was then confirmed as a true energy minimum using vibrational frequency data to verify its stability. Electronic and optical properties were investigated using frontier molecular orbital (FMO) analysis and time-dependent DFT (TD-DFT) calculations to evaluate electronic transitions and charge-transfer behavior.

Molecular electrostatic potential (MEP) was calculated to identify electron-rich and electron-deficient reactive regions, and global reactivity descriptors were analyzed to describe molecular stability and chemical reactivity. In addition, the NLO parameters were determined to analyze the electronic polarization properties of gefitinib.

NCI and reduced density gradient (RDG) analyses were also performed to visualize weak intramolecular interactions and steric effects within the molecular structure. The obtained results provide comprehensive insight into the structural, electronic, spectroscopic, and reactive characteristics of gefitinib. The calculated HOMO–LUMO energy gap and global reactivity descriptors suggest good kinetic stability and moderate sensitivity to intramolecular charge transfer.

2. Methodology

All quantum chemical simulations were carried out using the Gaussian 09 program package [7,8]. The molecular geometry of gefitinib was optimized within the framework of density functional theory (DFT), employing the B3LYP exchange–correlation functional in combination with the 6-311G(d,p) basis set [9–11]. The optimization process was performed without imposing any symmetry restrictions, allowing the molecule to attain its lowest-energy configuration on the potential energy surface.

To verify the nature of the optimized structure, harmonic vibrational frequency calculations were performed at the same level of theory. The absence of imaginary frequencies confirmed that the structure corresponded to a true minimum [12]. These calculations also provided infrared (IR) intensities and Raman activities, which were used to interpret the vibrational behavior of the molecule [13].

The electronic structure was further explored through frontier molecular orbital (FMO) analysis, focusing on the HOMO and LUMO obtained from the converged wavefunction [14]. In addition, the density of states (DOS) profile was generated using the GaussSum program to examine the distribution of energy levels among the molecular orbitals [15].

To investigate the charge distribution and chemically active regions, molecular electrostatic potential (MEP) surfaces were mapped [16]. Global reactivity parameters, including chemical potential, hardness, softness, and the electrophilicity index, were evaluated using frontier orbital energies within the conceptual DFT framework [17,18].

NLO properties, such as the dipole moment, polarizability, and first hyperpolarizability, were determined using the finite-field approach available in Gaussian 09 [19], providing insight into the response of the molecule to an applied electric field.

Finally, weak intramolecular interactions were analyzed using RDG analysis in combination with the NCI method [20]. This approach enables the identification and visualization of van der Waals interactions, hydrogen bonding, and steric effects that contribute to molecular stability.

3. Results and Discussion

3.1. Molecular Structure Optimization and Analysis

The molecular geometry of gefitinib was optimized using density functional theory (DFT) with the B3LYP exchange–correlation functional in combination with the 6-311G(d,p) basis set, as implemented in the Gaussian 09 program package. The optimization was carried out without imposing any symmetry restrictions, allowing the molecule to attain its lowest-energy configuration on the potential energy surface. The convergence criteria for energy and forces were satisfactorily met within the default thresholds of the Gaussian program, confirming that the optimized structure corresponds to a stable equilibrium configuration (Figure 1).

The total electronic energy of the optimized structure was calculated to be −1857.8527 a.u. The dipole moment of the molecule was found to be 5.26 D, with components of μx = 4.66 D, μy = 2.09 D, and μz = 1.26 D along the respective Cartesian axes. The relatively large dipole moment indicates significant charge separation within the molecular framework, primarily arising from the presence of heteroatoms and electron-withdrawing functional groups. This uneven distribution of electron density contributes to the overall polarity of the molecule, which may significantly influence its intermolecular interactions and potential biological activity.

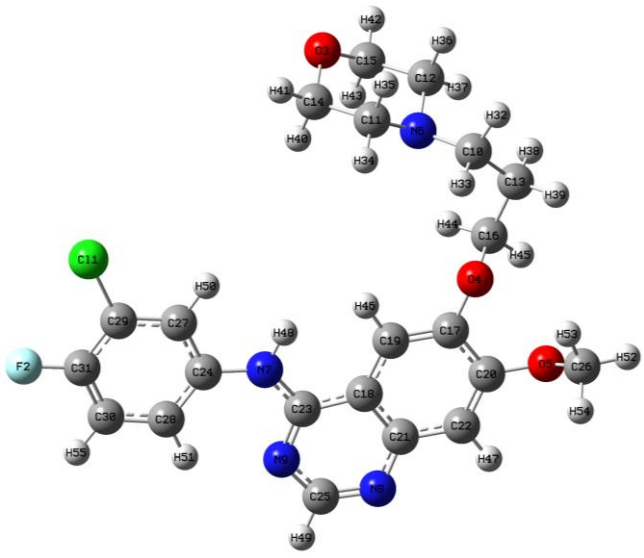

Fig. 1. Optimized structure of Gefitinib molecule.

3.2. Vibrational Properties and Frequency Analysis

Vibrational analysis provides valuable insight into the functional groups and structural features present in the optimized molecular geometry. The simulated IR and Raman spectra are presented in Figures 2 and 3, respectively, and display several characteristic bands corresponding to various stretching and deformation modes associated with the aromatic rings, heterocyclic quinazoline core, and aliphatic substituents.

The high-frequency region of the spectrum is dominated by N-H and C-H stretching vibrations. A broad band observed around 3400 cm-1 can be attributed to N-H stretching vibrations associated with the amine group present in the quinazoline framework. Aromatic and aliphatic C-H stretching modes appear in the region of 2956-2808 cm-1, arising from the alkyl and aromatic hydrogen atoms attached to the carbon skeleton.

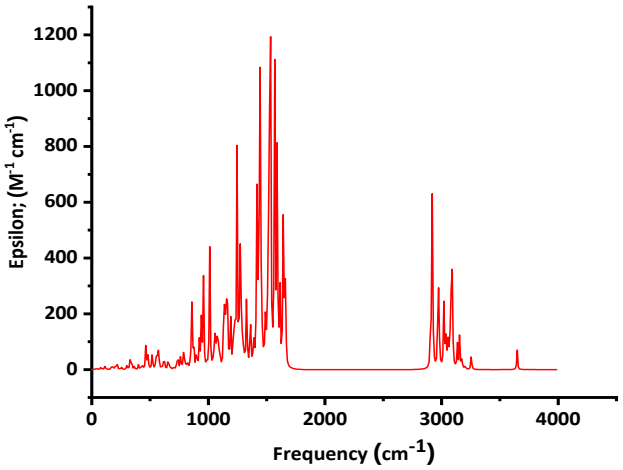

Fig. 2. IR graph of Gefitinib molecule.

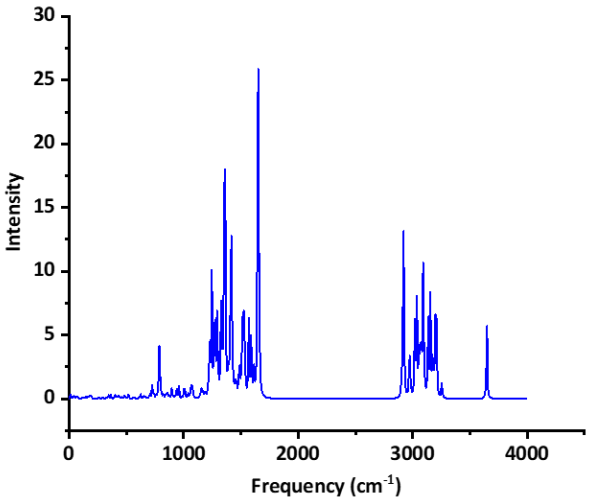

Fig. 3. Raman Activity Spectrum of Gefitinib molecule.

In the mid-frequency region, several prominent bands are observed that correspond to ring vibrations and heteroatom stretching modes. The strong band near 1625 cm-1 is assigned to C=N stretching vibrations within the quinazoline heterocyclic ring system. Another intense band appearing at 1578 cm-1 corresponds to aromatic C=C stretching vibrations, which are characteristic of conjugated aromatic systems. A significant peak at 1530 cm-1 is also attributed to aromatic C=C skeletal stretching, confirming the presence of the conjugated ring structure in the molecule.

Additional bands appearing around 1500 cm-1 and 1472 cm-1 are associated with aromatic ring deformation and C-H bending vibrations. The peak observed at 1429 cm-1 can be assigned to C-N stretching vibrations, while the band near 1398 cm-1 is related to C-H bending modes of the aromatic framework [21-22].

In the lower frequency region, several bands correspond to heteroatom–carbon vibrations and skeletal modes. The absorption peaks around 1227 cm-1 and 1219 cm-1 are attributed to C-O stretching vibrations associated with the methoxy, and ether groups present in the molecular structure. The strong band appearing at 1110 cm-1 corresponds to C-O-C stretching vibrations within the ether linkage.

The detailed vibrational assignments are summarized in Table 1, which lists the calculated frequencies along with their corresponding molecular vibrations.

Table 1. Theoretical vibrational frequencies (cm-1) and corresponding assignments for the gefitinib molecule.

Frequency (cm^{-1})	Assignment
3400	N—H stretching
2956	Aromatic/aliphatic C—H stretching
2921	Aliphatic C—H stretching
2808	C—H stretching
1649	C =N stretching
1625	C =N ring stretching
1578	Aromatic C =C stretching
1530	Aromatic ring stretching
1500	Aromatic C—H bending
1472	Ring deformation
1429	C—N stretching
1398	C—H bending
1227	C—O stretching
1110	C—O—C stretching
1028	C—F stretching
847	Aromatic C—H out-of-plane
542	Ring deformation

Furthermore, the peak around 1028 cm-1 can be assigned to C-F stretching vibrations, which arise due to the presence of the fluorine substituent on the aromatic ring. Lower-frequency bands observed at 847 cm-1 and 542 cm-1 correspond to out-of-plane aromatic C-H bending and ring deformation modes, respectively.

The vibrational modes calculated for C-O, C-F, and for aromatic ring deformations also agreed with the experimental spectral features reported for gefitinib. Minor deviations between theoretical and experimental frequencies may arise from anharmonic vibrational effects, intermolecular interactions, and the difference between isolated gas-phase calculations and condensed-phase experimental measurements [23].

The good agreement between the calculated and experimental vibrational spectra indicates the reliability of the B3LYP/6-311G(d,p) level of theory employed in the present investigation for describing the structural and spectroscopic properties of gefitinib.

3.3. UV-Visible Absorption Analysis

The electronic absorption characteristics of gefitinib were characterized by the time-dependent density functional theory (TD-DFT) calculations at the theory's B3LYP/6-311G(d,p) level. UV-Visible spectra enable important information on the electronic excitation response, frontier molecular orbital engagement and intramolecular charge transfer of the molecular system.

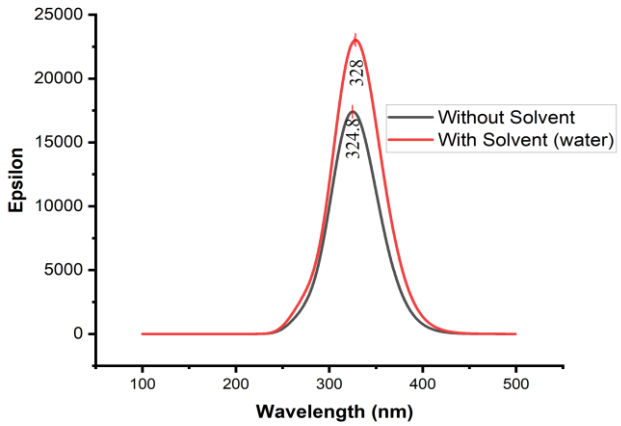

Fig. 4. UV-Vis Spectrum of Gefitinib molecule.

Visualisation of the calculated UV-Visible absorption spectra of gefitinib in gas and aqueous media is given in Figure 4. Solvent effects were included according to the Polarizable Continuum Model (PCM) with water as solvent. The observed spectrum demonstrates a significant absorption band at about 325 nm, strongly related to $\pi \longrightarrow \pi^*$ electronic transitions in the conjugated aromatic and quinazoline structure of the molecule. The transition is predominantly related to electron excitation from the highest occupied molecular orbital (HOMO) to the lowest unoccupied molecular orbital (LUMO). Electron-donating and electron-withdrawing substituent groups localized to the quinazoline ring increase π-electron delocalization around the molecule and thereby improve electronic excitation and charge shifting. Other absorption bands present, which lie in the wavelength range from 260-300 nm, are largely ascribed to $\pi \longrightarrow \pi^*$ transitions involving aromatic carbon–carbon groups and heterocyclic moieties of the molecule. Weak absorption features at the wavelength range of 220-240 nm can be attributed to transition $n \longrightarrow \pi^*$ associated with the lone pair electrons in nitrogen and oxygen atoms [24].

Table 2. Theoretical UV-Visible absorption bands and electronic transition assignments for gefitinib.

Medium	λ_{max} (nm)	Major Transition	Assignment
Gas phase	~320-325	HOMO⟶LUMO	$\pi \longrightarrow \pi^*$
Water (PCM)	Slightly higher λ_{max}	HOMO⟶LUMO	$\pi \longrightarrow \pi^*$ with solvent stablization
Higher-energy bands	220-290	HOMO-1⟶LUMO	$n \longrightarrow \pi^*$

These transitions require relatively higher excitation energies and therefore appear at shorter wavelengths. Comparison of the gas-phase and solvent-phase spectra reveals a slight bathochromic/red shift of the principal absorption band in aqueous medium, as shown in Table 2. This shift can be attributed to the stabilization of the excited electronic states by the polar solvent environment, which slightly lowers the excitation energy. Such behavior is characteristic of the electronic distribution of gefitinib and reflects its response to solvent-induced polarization. The electronic transitions indicate pronounced π-electron delocalization within the aromatic and heterocyclic rings, which contributes to the stabilization of the electronic structure and promotes intramolecular charge transfer.

The absorption band observed at around 325 nm for gefitinib is in good agreement with previous experimental UV–Visible reports, in which two intense absorption peaks were recorded at 331 and 345 nm in ethanol medium [23]. Minor discrepancies between theoretical and experimental wavelengths may arise from solvent effects, vibronic interactions, and the inherent approximations associated with the DFT functional and basis set used in the calculations.

These results are also consistent with the frontier molecular orbital analysis and support the conjugated nature of the gefitinib molecular framework. In conclusion, the UV–Visible spectral analysis highlights the critical role of the quinazoline core and the associated substituent groups in determining the electronic and optical properties of gefitinib, which may influence its photophysical behavior and potential optoelectronic applications.

3.4. Density of States (DOS) Analysis

DOS analysis provides essential information about occupied and unoccupied molecular orbitals and their contributions to the overall electronic behavior. The obtained DOS spectrum clearly separates the occupied valence region from the unoccupied conduction region [25].

The highest occupied molecular orbital (HOMO) and the lowest unoccupied molecular orbital (LUMO) were calculated to be −6.0734 eV and −1.8243 eV, respectively, resulting in an energy gap of 4.2491 eV. The large HOMO–LUMO energy gap indicates good kinetic stability and a moderate intramolecular charge transfer character of the molecule within its conjugated framework. Frontier orbital analysis further reveals that the major electronic contributions originate from π orbitals localized on the aromatic rings and the quinazoline heterocyclic core, while heteroatoms such as nitrogen and oxygen also contribute to the electronic distribution.

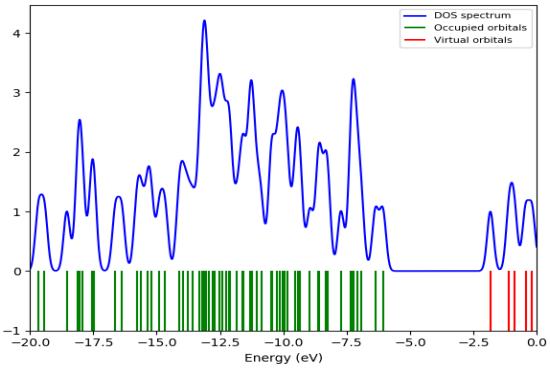

Fig. 5. Density of States (DOS) spectrum of gefitinib calculated at the B3LYP/6-311G(d,p) level of theory, showing the distribution of occupied and unoccupied molecular orbitals and the HOMO-LUMO energy gap.

The observed orbital distribution indicates widespread π-electron delocalization throughout the molecular network, which is of significant importance for the optical and electronic properties of gefitinib. As shown in Figure 5, the electronic states within the frontier orbital region are relatively closely spaced, so that it is likely that intramolecular charge redistribution occurs between electron-rich aromatic sections and electron-deficient heteroatomic regions. These electronic interactions are consistent with frontier molecular orbital and UV-Visible spectral analyses, indicating moderate intramolecular charge transfer in the molecule in general.

On the whole, the DOS analysis is in line with the reported existence of an extended conjugated electronic system for gefitinib and further elucidates the electronic distribution which controls both structural rigidity and spectroscopic performance.

3.5. FMO, MEP, and Global Reactivity Descriptor Analysis

Frontier molecular orbital (FMO) analysis was conducted to investigate the molecular structure, charge-transfer behavior, and chemical reactivity of gefitinib. The highest occupied molecular orbital (HOMO) and the lowest unoccupied molecular orbital (LUMO) are particularly important for understanding the electron-donating and electron-accepting properties of the molecule, since these frontier molecular orbitals are strongly associated with molecular excitation and intermolecular interactions [26].

The calculated HOMO and LUMO energies at the B3LYP/6-311G(d,p) level of theory were −6.0734 eV and −1.8243 eV, respectively, resulting in a HOMO–LUMO energy gap of 4.2491 eV, as presented in Figure 6. The relatively large energy gap indicates good kinetic stability and moderate intramolecular charge-transfer capability. These electronic characteristics can be attributed to the conjugated nature of the molecular framework, particularly the aromatic systems and heteroatomic substituents.

The Global Reactivity Descriptor analysis is shown in Table 3. The calculated chemical potential was −3.9488 eV, indicating the tendency of the molecule to attract electrons. The chemical hardness was found to be 2.1246 eV, while the corresponding chemical softness was 0.2353 eV^{-1}. The relatively moderate hardness value suggests that the molecule exhibits a balanced relationship between stability and reactivity.

Furthermore, the electrophilicity index was calculated to be 3.6697 eV, indicating that gefitinib possesses a considerable ability to accept electrons during chemical interactions. The maximum electronic charge-transfer value of 1.8587 further supports the potential of the molecule to participate in charge-transfer processes.

The spatial orientation of the frontier orbitals indicates that the HOMO is largely concentrated around the aromatic rings and nitrogen heterocyclic regions, a clear representation of electron-rich areas of the molecule. The LUMO, on the other hand, is primarily distributed into the quinazoline core and adjacent substituent groups, indicating a preferential distribution of electrons through that unit. This observed orbital separation may imply potential intramolecular charge redistribution from electron-rich aromatic regions to electron-deficient heteroatomic regions upon electronic excitation.

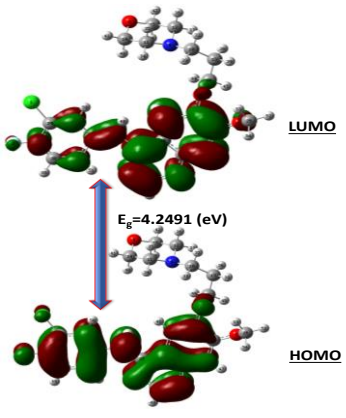

Fig. 6. Frontier molecular orbitals of gefitinib calculated at the B3LYP/6-311G(d,p) level of theory.

Table 3. Global reactivity parameters of Gefitinib molecule.

HOMO (eV)	LUMO (eV)	Chemical Potential μ (eV)	Chemical Hardness η (eV)	Electrophilicity Index ω (eV)	Softness S (eV^{-1})	Energy Gap E_g (eV)	Maximum Electronic Charge Transfer ΔN_{max}
-6.0734	-1.8243	-3.9488	2.1246	3.6697	0.2353	4.2491	1.8587

Table 4. Calculated polarizability and hyperpolarizability tensor components of the gefitinib molecule at the B3LYP/6-311G(d,p) level of theory.

Nonlinear Optical Parameters	Value (~~in~~ a.u.)	$\alpha\times 10^{-24}$ and $\beta\times 10^{-33}$ (~~in~~ esu)
$\Delta\alpha$	227.6548	33.7384
$\alpha_{Isotropic}$	313.2200	46.4192
α_{xx}	429.1343	63.5977
α_{xy}	8.2345	1.2203
α_{yy}	328.1376	48.6300
α_{xz}	4.5677	0.6769
α_{yz}	42.4157	6.2860
α_{zz}	182.3882	27.0299
β_{Total}	1361.6429	11763.6419
β_{xxx}	1099.7474	9500.9378
β_{xxy}	-603.5153	-5213.8892
β_{xyy}	-30.7779	-265.8964
β_{yyy}	-115.6183	-998.8497
β_{xxz}	-140.3912	-1212.8676
β_{xyz}	-44.3313	-382.9866
β_{yyz}	-59.8287	-516.8720
β_{xzz}	97.1363	839.1803
β_{yzz}	26.4688	228.6694
β_{zzz}	79.8697	690.0101

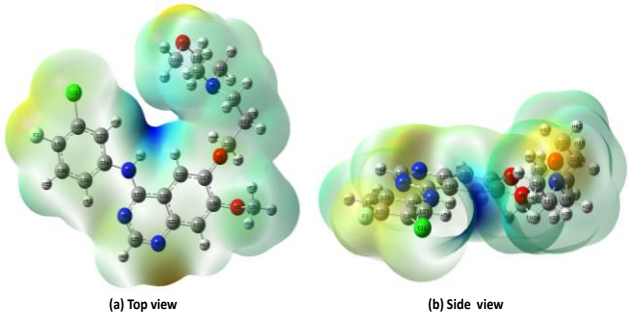

Fig. 7. Molecular electrostatic potential (MEP) surface of gefitinib showing electron-rich (red) and electron-deficient (blue) regions.

As a second step towards investigating charge distribution and the reactive regions of the molecule, the molecular electrostatic potential (MEP) surface was generated based on the optimized geometry. The MEP map is a graphical representation of the electrostatic potential distribution across the molecular surface and is useful for identifying electrophilic and nucleophilic reactive sites. The MEP surface exhibits regions of negative electrostatic potential, shown in red, which correspond to electron-rich regions mainly localized around oxygen and nitrogen atoms, owing to their high electronegativity. Positive electrostatic potential domains, shown in blue, on the other hand, are largely localized around hydrogen atoms and some peripheral carbon atoms, signifying relatively electron-deficient regions [27]. Heteroatoms, as shown in Figure 7, play an important role in the molecule's intermolecular properties and local charge distributions within the molecule.

In addition to the FMO analysis, also referred to as global reactivity descriptors were determined by means of the HOMO and LUMO energy in the conceptual density functional theory. These descriptors quantify the stability, electronic softness, electrophilicity and chemical reactivity of the molecular characteristics of the gefitinib molecule.

3.6. Nonlinear Optical Properties Analysis

The nonlinear optical (NLO) properties of the gefitinib molecule were evaluated using the B3LYP functional in conjunction with the 6-311G(d,p) basis set. The polarizability and hyperpolarizability tensors were obtained directly from the Gaussian output based on the finite-field approach. All computed NLO parameters were initially expressed in atomic units (a.u.) and subsequently converted to esu.

The finite-field method is based on a Taylor series expansion of the total energy of the system in the presence of an external electric field, as described by Kurtz et al. [28,29]. The energy *E(F)* and dipole moment μ_i *(F)* can be expressed as:

$$E(F) = E(0) - \mu F_i - \frac{1}{2!}\alpha_{ij}F_iF_j - \frac{1}{3!}\beta_{ijk}F_iF_jF_k - \frac{1}{4!}\gamma_{ijkl}F_iF_jF_kF_l - \ldots\ldots\ldots\ldots \quad (1)$$

$$\mu_i(F) = \mu_i(0) + \alpha_{ij}F_j + \frac{1}{2!}\beta_{ijk}F_jF_k + \frac{1}{3!}\gamma_{ijkl}F_jF_kF_l + \ldots\ldots\ldots\ldots\ldots \quad (2)$$

where E(0) is the energy of the molecule in the absence of an external electric field, $\mu_i(0)$ is its permanent i^{th} dipole moment, α_{ij} is the dipole polarizability, and β_{ijk} and γ_{ijkl} are the first- and second-order hyperpolarizabilities.

The isotropic polarizability α is described by a second-rank tensor, whereas the first β and second γ order polarizability are represented by higher-rank tensors with many components.

The isotropic polarizability is calculated as the mean value as given in the following equation [30-33]:

$$\langle\alpha\rangle = \frac{1}{3}(\alpha_{xx} + \alpha_{yy} + \alpha_{zz}) \quad (3)$$

And the polarizability anisotropy invariant is:

$$\Delta\alpha = \left[\frac{(\alpha_{xx} - \alpha_{yy})^2 + (\alpha_{yy} - \alpha_{zz})^2 + (\alpha_{zz} - \alpha_{xx})^2}{2}\right]^{\frac{1}{2}} \quad (4)$$

The total static first hyperpolarizability β was obtained from the relation:

$$\beta_{tot} = \sqrt{(\beta_x^2 + \beta_y^2 + \beta_z^2)} \quad (5)$$

Upon calculating the individual static components,

$$\beta_i = \frac{1}{3}\sum_{k=x,y,z}(\beta_{ikk} + \beta_{kik} + \beta_{kki}); \quad where\ i = x, y, z \quad (6)$$

Due to the Kleinman symmetry:

$$\beta_{xyy} = \beta_{yxy} = \beta_{yyx}\ ;\ \beta_{yyz} = \beta_{yzy} = \beta_{zyy}\ , \ldots\ldots$$

We can finally obtain the equation that has been employed:

$$\beta_{tot} = \sqrt{(\beta_{xxx} + \beta_{xyy} + \beta_{xzz})^2 + (\beta_{yyy} + \beta_{yzz} + \beta_{yxx})^2 + (\beta_{zzz} + \beta_{zxx} + \beta_{zyy})^2} \quad (7)$$

Table 4 shows the calculated NLO parameters of gefitinib. Both the isotropic polarizability and first hyperpolarizability values indicate that the molecule possesses appreciable electronic polarization characteristics. The relatively high polarizability can be attributed to the presence of an extended π-conjugated system, together with heteroatoms incorporated within the quinazoline framework.

The aromatic rings and heteroatomic substituents facilitate the redistribution of electron density under an external electric field, thus contributing to the overall molecular polarization. In particular, the presence of electron-rich and electron-deficient regions in the molecular framework facilitates intramolecular charge

transfer, which plays an important role in determining the nonlinear optical response of the molecule.

The calculated first hyperpolarizability suggests that gefitinib exhibits moderate nonlinear optical activity due to π-electron delocalization and structural asymmetry. Conjugated molecular pathways establish donor–acceptor interactions, thereby enhancing electronic communication across the molecule and contributing to the observed hyperpolarizability values.

The calculated first hyperpolarizability of gefitinib was found to be considerably larger than that of urea, a commonly used reference NLO material. The obtained β_{total} value is approximately 31 times higher than the reported hyperpolarizability of urea ($\beta=0.3728\times10^{-30}$ esu$=372.8\times10^{-33}$ esu), [34] indicating appreciable nonlinear optical response arising from extended π-conjugation and intramolecular charge transfer within the molecular framework.

While gefitinib is known as an anticancer therapeutic agent, the present theoretical study suggests that the molecule possesses promising electronic response properties. These results indicate that heteroatomic aromatic frameworks in conjugated pharmaceutical molecules may exhibit useful optical polarization behavior relevant to molecular optoelectronic research.

3.7. NCI and RDG Analysis

The non-covalent interaction (NCI) analysis was performed to investigate weak intermolecular and intramolecular interactions within the gefitinib molecule using the reduced density gradient (RDG) approach. A variety of interactions (e.g., van der Waals forces, steric effects, and weak attractive interactions) are instrumental in modulating molecular stability, conformational effects, and intermolecular recognition systems. RDG analysis was conducted by plotting the reduced density gradient as a function of sign(λ2)ρ, where λ2 is the second eigenvalue of the electron-density Hessian matrix. This allows to identify attractive and repulsive interaction structures in the molecular system [35,36].

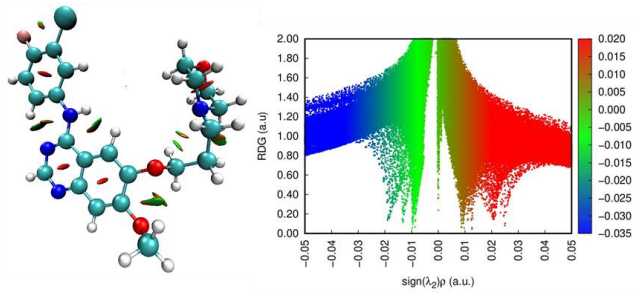

Fig. 8. NCI isosurface and RDG scatter plot of the gefitinib molecule illustrating non-covalent interactions. Blue, green, and red regions correspond to attractive interactions, van der Waals interactions, and steric repulsion, respectively.

The RDG scatter plot, along with the NCI isosurface of gefitinib, is presented in Figure 8. As shown in Figure 8, negative sign(λ_2)ρ values correspond to attractive interactions, near-zero values indicate weak van der Waals interactions, and positive values represent steric repulsion. The NCI isosurface was constructed using an RDG isovalue of 0.5 a.u., with blue, green, and red regions corresponding to attractive interactions, weak dispersive interactions, and steric repulsion, respectively. The NCI surface shows many green regions surrounding the aromatic rings and heteroatomic substituent regions, suggesting weak van der Waals interactions within the conjugated molecular structure. These interactions stabilize the molecular conformation and are prominent in the quinazoline heterocyclic region and nearby aromatic moieties [37,38].

Small blue areas near nitrogen and oxygen atoms indicate weak attractive interactions in localized electron-rich centers. Such interactions may influence intermolecular recognition behavior and may affect the binding features of the molecule in biological environments. In contrast, the presence of red-colored regions in localized portions of the molecular surface is associated with steric repulsion owing to the proximity of atomic contacts in neighboring substituent groups.

These steric interactions contribute to maintaining the three-dimensional molecular geometry and spatial arrangement of the substituents. In conclusion, the RDG and NCI analyses clearly indicate that both weak dispersive interactions and localized attractive interactions strongly affect the conformational stability and electronic organization of the gefitinib molecule.

4. Conclusions

This study conducted a comprehensive quantum chemical investigation of the anticancer drug gefitinib using density functional theory (DFT) at the B3LYP/6-311G(d,p) level of theory. Vibrational frequency analysis confirmed that the optimized molecular geometry represents a true minimum-energy structure.

The IR and Raman spectra were found to reproduce all the characteristic vibrational features of the quinazoline framework and associated functional groups, showing reasonable agreement with experimental studies. TD-DFT UV–Visible analysis revealed that the main absorption bands mainly originate from π⟶π* transitions within the electronic structure of the conjugated aromatic system. The inclusion of solvent effects using the PCM water model induced a small bathochromic shift in the absorption spectrum, indicating the stabilization of the excited electronic states in a polar solution.

Frontier molecular orbital analysis showed HOMO and LUMO energies of −6.0734 eV and −1.8243 eV, respectively, with a HOMO–LUMO energy gap of 4.2491 eV. The computed energy gap indicates satisfactory kinetic stability as well as moderate intramolecular charge-transfer character. The mapping of the molecular electrostatic potential (MEP) surface indicated that electron-rich regions are mainly concentrated around the nitrogen and oxygen atoms, indicating potential sites for

intermolecular interactions. The evaluated global reactivity descriptors also confirmed the electronic stability of the molecule and its moderate electrophilic character.

DOS analysis also provided further insight into the electronic distribution across the frontier orbital region and provided evidence for π-electron delocalization as a key factor controlling the electronic properties of gefitinib. Nonlinear optical (NLO) parameters were calculated, revealing significant molecular polarizability and first hyperpolarizability due to the increased π-conjugation and asymmetric distribution of electrons.

Moreover, NCI and RDG analyses showed that, in addition to weak van der Waals interactions, favorable local attractive interactions and steric effects are also present, contributing to the conformational stability of the molecule. Therefore, the current study provides detailed insight into the structural, spectroscopic, electronic, and reactive properties of gefitinib. This approach not only demonstrates the capability of quantum chemical methods to improve our understanding of biologically relevant heterocyclic systems, but may also provide a useful theoretical foundation for future investigations into pharmaceutical reactivity and molecular optoelectronic applications.

Acknowledgements

The authors gratefully acknowledge the Central Laboratory, Department of Physics, University of Lucknow, for providing the necessary computational facilities and research infrastructure to carry out this work.

Funding Statement

The authors declare that no specific funding was received for this research work.

Conflicts of Interest

The authors declare no conflict of interest.

Authors' Contributions

Atul Kumar Shukla: Investigation, Visualization, Writing-original draft, Writing-review & editing. Anchal Srivastava: Validation, review & editing. Sunil Kumar Mishra: Literature survey & Formal analysis. Mritunjai Mishra: Computational methodology, Data Validation, Visualization, Formal analysis & interpretation. Nitin Dwivedi: Validation, review & editing. R. K. Shukla: Conceptualization, Supervision, Resources, Formal analysis, review & editing.

References

[1] Gridelli, C., Rossi, A., Carbone, D. P., Guarize, J., Karachaliou, N., Mok, T., ... & Rosell, R. 2015. Non-small-cell lung cancer. *Nature reviews Disease primers*, 1(1), p.15009.

[2] Hendriks, L. E., Remon, J., Faivre-Finn, C., Garassino, M. C., Heymach, J. V., Kerr, K. M., ... & Reck, M. 2024. Non-small-cell lung cancer. *Nature Reviews Disease Primers*, 10(1), p.71.

[3] Ke, X., & Shen, L. 2017. Molecular targeted therapy of cancer: The progress and future prospect. *Frontiers in Laboratory Medicine*, 1(2), pp.69-75.

[4] Kris, M. G., Natale, R. B., Herbst, R. S., Lynch Jr, T. J., Prager, D., Belani, C. P., ... & Kay, A. C. 2003. Efficacy of gefitinib, an inhibitor of the epidermal growth factor receptor tyrosine kinase, in symptomatic patients with non–small cell lung cancer: a randomized trial. *Jama*, 290(16), pp.2149-2158.

[5] Penne, K., Bohlin, C., Schneider, S., & Allen, D. 2005. Gefitinib (IressaTM, ZD1839) and tyrosine kinase inhibitors: the wave of the future in cancer therapy. *Cancer nursing*, 28(6), pp.481-486.

[6] Srivastava, A. K., & Misra, N. 2021. DFT based studies on bioactive molecules. Bentham Science Publishers.

[7] Frisch, A. 2009. Gaussian 09W Reference. Wallingford, USA, 25p 470(4).

[8] Frisch, M. J., Trucks, G. W., Schlegel, H. B., Scuseria, G. E., Robb, M. A., Cheeseman, J. R., ... & Nakatsuji, H. 2009. Uranyl extraction by N, N-dialkylamide ligands studied by static and dynamic DFT simulations. *Gaussian*, 9(9), p.227.

[9] Becke, A. D. 1993. Density-functional thermochemistry. III. The role of exact exchange. *The Journal of chemical physics*, 98(7), pp.5648-5652.

[10] Lee, C., Yang, W., & Parr, R. G. 1988. Development of the Colle-Salvetti correlation-energy formula into a functional of the electron density. *Physical review B*, 37(2), p.785.

[11] Almlof, J., Helgaker, T., & Taylor, P. R. 1988. Gaussian basis sets for high-quality ab initio calculations. *The Journal of Physical Chemistry*, 92(11), pp.3029-3033.

[12] Porezag, D., & Pederson, M. R. 1999. Optimization of Gaussian basis sets for density-functional calculations. *Physical Review A*, 60(4), p.2840.

[13] Tikaram, Kumar, R., Kumar, Y. and Kumar, N. 2026. Physical, Electro-Optical, and Spectroscopic Properties of I52 liquid crystal: A Computational Study. *Progress in Physics of Applied Materials*, 6(4), pp.315-330.

[14] Sucheta, M., Pramod, A. G., Zikriya, M., Salma, K. M., Venugopal, N., Chaithra, R., ... & Murthy, S. 2022. Frontier molecular orbital, molecular structure and Thermal properties of 2, 4, 6, 8-tetramethyl-2, 3, 6, 7-tetrahydro-s-indacene-1, 5-dione using DFT calculation. *Materials Today: Proceedings*, 62, pp.5241-5244.

[15] Bayrakdar, A., Kart, H. H., Elçin, S., Ashfaq, M., Mali, S. N., Yasin, H. K. A., & Smerat, A. 2025. Concise experimental and DFT study of newly synthesized 5, 17-di (2-antracenylazo)-25, 27-[1, 3-ethylene-bis (aminocarbonylmethoxy)]-26, 28-dihydroxycalix [4] arene. *Chemical Physics Impact*, 11, p.100965.

[16] Priya, M. K., Revathi, B. K., Renuka, V., Sathya, S., & Asirvatham, P. S. 2019. Molecular structure, spectroscopic (FT-IR, FT-Raman, 13C and 1H NMR) analysis, HOMO-LUMO energies, Mulliken, MEP and thermal properties of

new chalcone derivative by DFT calculation. *Materials Today: Proceedings*, 8, pp.37-46.

[17] Ramirez-Balderrama, K., Orrantia-Borunda, E., & Flores-Holguin, N. 2017. Calculation of global and local reactivity descriptors of carbodiimides, a DFT study. *Journal of Theoretical and Computational Chemistry*, 16(03), p.1750019.

[18] Chattaraj, P. K., Nath, S., & Maiti, B. 2003. Reactivity descriptors. *Computational medicinal chemistry for drug discovery*, 11, p.295.

[19] Liyanage, P. S., de Silva, R. M., & de Silva, K. N. 2003. Nonlinear optical (NLO) properties of novel organometallic complexes: high accuracy density functional theory (DFT) calculations. *Journal of Molecular Structure: THEOCHEM*, 639(1-3), pp.195-201.

[20] Sarala, S., Geetha, S. K., Muthu, S., & Irfan, A. 2021. Computational investigation, comparative approaches, molecular structural, vibrational spectral, non-covalent interaction (NCI), and electron excitations analysis of benzodiazepine derivatives. *Journal of Molecular Modeling*, 27(9), p.266.

[21] Marković, J. M. D., Marković, Z. S., Krstić, J. B., Milenković, D., Lučić, B., & Amić, D. 2013. Interpretation of the IR and Raman spectra of morin by density functional theory and comparative analysis. *Vibrational spectroscopy*, 64, pp.1-9.

[22] Gautam, V., Mishra, M., Thapa, K. B., Kumar, J., Singh, D., & Kumar, D. 2023. Electronic, optical and spectroscopic properties of N-dialkyl-imidazolium hexafluorophosphate (CN MIM. PF6) ionic liquid crystal molecules investigated by computational methods. *Journal of Molecular Modeling*, 29(9), p.274.

[23] Rahman, A. M., Korashy, H. M., & Kassem, M. G. 2014. Gefitinib. *Profiles of drug substances, excipients and related methodology*, 39, pp.239-264.

[24] Ganiev, B., Mardonov, U., & Kholikova, G. 2023. Molecular structure, HOMO-LUMO, MEP-Analysis of triazine compounds using DFT (B3LYP) calculations. *Materials Today: Proceedings*.

[25] Toriyama, M. Y., Ganose, A. M., Dylla, M., Anand, S., Park, J., Brod, M. K., ... & Snyder, G. J. 2022. How to analyse a density of states. *Materials today electronics*, 1, p.100002.

[26] Hussein, H. A. 2023. A DFT study of structural-stability, Mulliken charges, MEP, FMO, and NLO properties of trans alkenyl substituted chalcones conformers: theoretical study. *Structural Chemistry*, 34(6), pp.2201-2223.

[27] Rawat, P., Singh, R. N., Ranjan, A., Ahmad, S., & Saxena, R. 2017. Antimycobacterial, antimicrobial activity, experimental (FT-IR, FT-Raman, NMR, UV-Vis, DSC) and DFT (transition state, chemical reactivity, NBO, NLO) studies on pyrrole-isonicotinyl hydrazone. *Spectrochimica Acta Part A: Molecular and Biomolecular Spectroscopy*, 179, pp.1-10.

[28] Kurtz, L. A., Smith, R. E., Parks, C. L., & Boney, L. R. 1978. A comparison of the method of lines to finite difference techniques in solving time-dependent partial differential equations. *Computers & Fluids*, 6(2), pp.49-70.

[29] Buckingham, A. D., & Orr, B. J. 1967. Molecular hyperpolarisabilities. *Quarterly Reviews, Chemical Society*, 21(2), pp.195-212.

[30] Mveme, C. D. D., Nya, F. T., Ejuh, G. W., Kamsi, R. A. Y., & Ndjaka, J. M. B. 2020. Density functional theory study of optoelectronic, nonlinear optical, piezoelectric and thermodynamic properties of poly (3, 4-ethylenedioxythiophene), poly (3, 4-ethylenedioxyselenophene) and their derivatives. *Optical and Quantum Electronics*, 52, pp.1-16.

[31] Kamsi, R. A. Y., Ejuh, G. W., Mkounga, P., & Ndjaka, J. M. B. 2020. Study of the molecular structure, electronic and chemical properties of Rubescin D molecule. *Chinese Journal of Physics*, 63, pp.104-112.

[32] Yossa Kamsi, R. A., Ejuh, G. W., Tchoffo, F., Mkounga, P., & Ndjaka, J. M. B. 2019. Electronic Structure, Spectroscopic (IR, Raman, UV-Vis, NMR), Optoelectronic, and NLO Properties Investigations of Rubescin E (C31H36O7) Molecule in Gas Phase and Chloroform Solution Using Ab Initio and DFT Methods. *Advances in Condensed Matter Physics*, 2019(1), p.4246810.

[33] Midoune, A., & Messaoudi, A. 2020. DFT/TD-DFT computational study of the tetrathiafulvalene-1, 3-benzothiazole molecule to highlight its structural, electronic, vibrational and non-linear optical properties. *Comptes Rendus. Chimie*, 23(2), pp.143-158.

[34] Kurtz, H. A., Stewart, J. J. P., & Dieter, K. M. 1990. Calculation of the nonlinear optical properties of molecules. *Journal of Computational Chemistry*, 11(1), pp.82–87.

[35] Johnson, E. R., Keinan, S., Mori-Sánchez, P., Contreras-García, J., Cohen, A. J., & Yang, W. 2010. Revealing noncovalent interactions. *Journal of the American Chemical Society*, 132(18), pp.6498-6506.

[36] Contreras-García, J., Johnson, E. R., Keinan, S., Chaudret, R., Piquemal, J. P., Beratan, D. N., & Yang, W. 2011. NCIPLOT: a program for plotting noncovalent interaction regions. *Journal of chemical theory and computation*, 7(3), pp.625-632.

[37] Tretiakov, S., Nigam, A., & Pollice, R. 2025. Studying noncovalent interactions in molecular systems with machine learning. *Chemical reviews*, 125(12), pp.5776-5829.

[38] Vengatesh, G., Vinushya, N., Jeyaprakash, G. M., Mohini, A., Mondal, P., Reddy, R., & Shriram, Z. O. 2025. Crystal structures, NCI-RDG, Hirshfeld surface and energy framework analysis of tetra aryl substitute bispidine and oxaquinuclidine core containing derivatives: A potential COVID-19 drug candidate. *Journal of Molecular Structure*, 1321, p.140202.